Performance optimization of an external enhancement resonator for optical second-harmonic generation

E. Jurdik, J. Hohlfeld, A. F. van Etteger, A. J. Toonen, W. L. Meerts, H. van Kempen, and Th. Rasing

Research Institute for Materials, University of Nijmegen, Toernooiveld 1, 6525 ED Nijmegen, The Netherlands

Received August 30, 2001; revised manuscript received November 26, 2001

We study the factors that ultimately limit the performance of an external enhancement resonator for optical second-harmonic generation (SHG). To describe the resonant SHG process we introduce a theoretical model that accounts for the intensity-dependent cavity loss that is due to harmonic generation and that also includes a realistic assumption about the shape and the frequency width of the laser mode. With the help of this model we optimized the performance of a doubling cavity based on a lithium triborate (LBO) crystal. This cavity was used for frequency doubling the output of a single-frequency titanium-doped sapphire laser at 850 nm. We were able to push the total second-harmonic conversion efficiency to 53% (a 1.54-W pump resulted in 820 mW of second-harmonic light), which to our knowledge is the best result ever reported for a LBO-based doubling cavity.

OCIS codes: 190.4360, 190.2620, 230.5750.

1. INTRODUCTION

Optical second-harmonic generation (SHG) is a technique of high technological relevance because it provides the means for extending laser radiation to shorter wavelengths of the optical spectrum. The main objective is to convert as large a fraction of the power at the fundamental frequency to that at the second harmonic. Since the first experimental demonstration of SHG by Franken *et al.*,[1] considerable progress in understanding the factors that lead to high conversion efficiencies has been made. In particular, it has been shown that the use of an optical resonator for fundamental or harmonic light or both results in a considerably more efficient SHG process. This strategy was proposed in the pioneering work of Armstrong *et al.*[2] and was investigated more thoroughly by Ashkin *et al.*[3]

SHG in an external resonator for the fundamental light—the so-called doubling cavity—is usually chosen when no laser source is available at the desired wavelength but there is a laser at the double wavelength. Another motivation for this choice is the fact that integration of a doubling cavity into a laser setup helps to make the system all-solid-state, with obvious advantages related to maintainance and compactness. In general, SHG in an external resonator is preferred there when any disturbance to the laser action as a result of placing a nonlinear, optically active crystal into the laser cavity (that also contains high intensities) must be prevented. We note that the feasibility requirement for efficient frequency doubling in an external resonator is a laser source with a single-frequency output. This implies that a doubling cavity is useful in applications such as high-resolution laser spectroscopy and atom optics. The concern is to select the best cavity configuration and to obtain the highest possible conversion efficiency with the lowest possible noise in the generated power.

A number of reports of frequency doubling in an external resonator appeared in the literature during the past decade (see, e.g., Refs. 4–8). Those reports have been motivated mostly by the need to extend the wavelength range of a single-frequency, cw titanium-doped sapphire (Ti:sapphire) laser. To this end, either a single doubling stage[4–6] or even two successive resonant cavities[7,8] were employed. Previous studies especially emphasized selection criteria for the nonlinear crystal and also for cavity geometry to maximize the Boyd–Kleinman focusing parameter.[9] The argument of those reports was based on the theory of an empty Fabry–Perot resonator in the steady-state regime. Within this framework the cavity loss that is due to depletion of the fundamental to second-harmonic (SH) radiation is accounted for as being due to a loss coefficient that does not change during the buildup of the intracavity field and so is independent of time. Although this procedure imitates the cavity performance at a given power, it leads to inconsistent results when one is modeling either the dependence of the cavity reflectivity and the SH conversion efficiency on the pump power or the transient behavior of these quantities.

In this paper we present an extensive theoretical and experimental study of SHG in an external enhancement resonator. We emphasize the physics of an optical resonator with a SHG crystal inside it. To describe the resonant SHG process we introduce a theoretical model based on a plane-wave approximation. It accounts for the intensity-dependent cavity loss that is due to harmonic generation and also includes a realistic assumption about the shape and the frequency width of the laser mode. We demonstrate that the behavior of a doubling cavity is correctly described only when both of these essential features are accounted for. To this end we compare the model to measurements with a lithium triborate (LBO-) based doubling cavity for SHG of a cw, single-frequency

Ti:sapphire laser at 850 nm. Excellent agreement between the model and the experiment is obtained. We show that only simultaneous measurements of both the power reflected from the doubling cavity and the generated power at the SH wavelength as functions of the incident power provide a key to the quantities that crucially influence the cavity performance. We optimized the total SH conversion efficiency at a 53% level (a 1.54-W pump resulted in 820 mW of SH light) with a projected efficiency of more than 70% at a laser power higher than that which is now available to us. It is worth remarking that the highest total conversion efficiency published so far is 40%.[8]

2. MODELING

An optical resonator is a device that allows light with only a distinct set of well-defined frequencies, or modes, to oscillate. A mode inside a resonator is supported because of constructive interference; it is in phase with itself after successive round trips. When an appropriate resonator configuration (mirrors, geometry, crystal, etc.) is chosen, the electric field amplitude of an optical wave can be considerably enhanced inside that resonator. It is this enhanced field amplitude that results in more-efficient SHG in a doubling cavity that resonates the fundamental light.

Our aim is to predict the enhancement factor for a given cavity layout and to calculate both the reflected fundamental and the generated SH power. In what follows, we assume that the optical fields are plane waves. In this approximation the longitudinal modes supported by the cavity are explicitly independent of the actual geometry (which dictates the transverse modes). For concreteness, however, we consider a four-mirror ring resonator with a nonlinear crystal for SHG inside it, as depicted schematically in Fig. 1. Mirror M1 with reflectivity R_1 (transmissivity $T_1 = 1 - R_1$) serves as the input coupler.[10] Intensity-independent losses that are not due to M1 are expressed here as reflectivity R_0. We note that R_0 includes losses associated with other cavity mirrors, with the crystal (excluding SHG) and, eventually, with some intracavity elements such as dust particles. Also, R_0 implicitly takes into account the geometry of the cavity (including possible misalignment).

To simplify the discussion of the intensity-dependent loss that is due to SHG from the crystal, we first assume a laser with a truly single-frequency output (infinitely sharp laser line). In this case the SH intensity $I_{\mathrm{SH}}(n)$ generated in the nth round trip of the fundamental wave in the cavity is quadratic in intracavity intensity $I_c(n)$:

$$I_{\mathrm{SH}}(n) = \alpha I_c^{\,2}(n). \tag{1}$$

Here α is the effective SH coefficient that accounts for all the details of the SHG process (the second-order susceptibility of the crystal, the crystal length, the profile of the transverse cavity mode, the walk-off angle of the fundamental and SH beams, phase matching, etc.). We mention that the simple formulation of Eq. (1) in terms of a single parameter α makes our treatment of SHG inside a resonator applicable to any cavity configuration. It now follows that the remaining intracavity intensity after the beam passes through the crystal is reduced to $T_{\mathrm{SH}}(n)I_c(n)$, where $T_{\mathrm{SH}}(n)$ denotes the intensity-dependent transmissivity of the crystal for the fundamental beam in the nth round-trip. It is given by

$$T_{\mathrm{SH}}(n) = 1 - \alpha I_c(n). \tag{2}$$

One must be aware of the fact that Eqs. (1) and (2) are an idealization. There might be deviations from these relations, especially in the case of high intracavity intensities. For example, the central part of the fundamental beam is depleted at a higher rate than its tails, and the transverse eigenmode of the cavity might change with time. Also, higher-order nonlinearities (which are due to, e.g., thermal and photorefractive processes) might influence the result. In these cases, Eqs. (1) and (2) would need to be corrected. In our experiment, however, we did not encounter any of these problems.

The intracavity field in the nth round trip $E_c(n)$ at the position of mirror M1 is given by[11]

$$E_c(n) = i\sqrt{T_1}E_i + \sqrt{R(n-1)}\exp(-i\phi)E_c(n-1), \tag{3}$$

where E_i is the fundamental field that is incident onto the cavity and ϕ is the phase acquired by the intracavity field in one round trip. Note that $\phi = 2\pi j$, where j is an integer, whenever the cavity is resonant with the incident field. The overall intensity loss in the nth round trip is $1 - R(n)$, where $R(n)$ reads as

$$R(n) = R_0 T_{\mathrm{SH}}(n) R_1. \tag{4}$$

In what follows, $R(n)$ is referred to as the overall intracavity reflectivity. The first term on the right-hand side of Eq. (3) represents the gain that is due to in-coupling and includes a phase shift of $\pi/2$ acquired in transmission through M1. The second term is the intracavity field in the previous round trip $E_c(n-1)$, corrected for the overall loss and phase accumulation in one round trip.

The fundamental reflected field $E_r(n)$ is derived by use of $E_c(n)$. Intracavity field $E_c(n)$ is first traced across the whole cavity and then transmitted through M1. After transmission, it recombines with the directly reflected beam. We therefore write

$$E_r(n) = -\sqrt{R_1}E_i - i[T_1 R(n)/R_1]^{1/2}\exp(-i\phi)E_c(n). \tag{5}$$

Optical intensities $I_c(n)$ and $I_r(n)$ associated with fields $E_c(n)$ and $E_r(n)$, respectively, are given by

$$I_{c,r}(n) = \tfrac{1}{2}\epsilon_0 c|E_{c,r}(n)|^2 \tag{6}$$

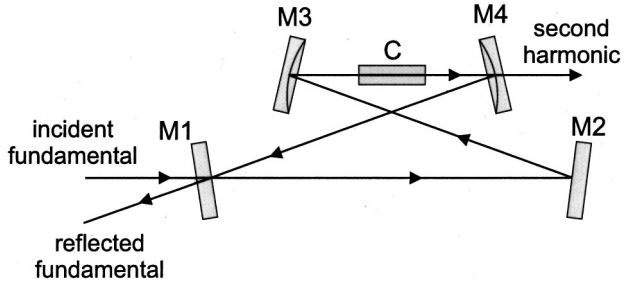

Fig. 1. Four-mirror ring cavity for SHG: M1, input coupler; M2–M4, cavity mirrors; C, nonlinear crystal.

where ϵ_0 is the permittivity of free space and c is the *in vacuo* speed of light.

Now the performance of a doubling cavity pumped with an infinitely sharp laser line can be predicted by solution of Eqs. (1)–(6), provided that α, R_0, and R_1 are known. Because intracavity field $E_c(n)$ is related to $R(n-1)$, it is instructive to distinguish the two cases of negligible and significant contributions of SHG to the total cavity loss. In the former case the overall intracavity reflectivity, $R(n) \simeq R_1 R_0 \equiv r$, is constant, and the steady-state intensities $I_c = I_c(n \to \infty)$ and $I_r = I_r(n \to \infty)$ are reduced to the familiar form

$$I_c = T_1 \frac{1}{1 + r - 2\sqrt{r}\cos(\phi)} I_i , \tag{7}$$

$$I_r = \left[R_1 + T_1 \frac{T_1 R_0 + 2r - 2\sqrt{r}\cos(\phi)}{1 + r - 2\sqrt{r}\cos(\phi)} \right] I_i , \tag{8}$$

respectively. Here I_i is the incident fundamental intensity. From Eqs. (7) and (8) we can see that both reflectivity $\rho = I_r/I_i$ and enhancement factor $\beta = I_c/I_i$ are independent of I_i. For a resonant cavity [$\cos(\phi) = 0$], the closer the value of R_1 is chosen to that of R_0, the larger is β. At $R_1 = R_0$ the loss-matching condition $\rho = 0$ is met and β is maximized. Consequently, the highest conversion efficiency $\eta = I_{SH}/I_i$ is expected for a loss-matched cavity. Moreover, because the maximum value of β increases with increasing R_0, the intensity-independent loss should be minimized to optimize the cavity performance. Doing so, however, would invalidate the assumption of negligible contribution of SHG to the total loss. Therefore, only a model that takes into account a significant contribution of SHG to the total loss correctly describes the performance of an optimized cavity. Overall intracavity reflectivity $R(n)$ then depends on intracavity intensity $I_c(n)$, and Eq. (3) has to be evaluated numerically. Reflected field E_r as well as intensities I_c and I_r are then calculated from Eqs. (5) and (6), respectively.

To illustrate the influence of the intensity-dependent loss on the performance of a doubling cavity, we show in Figs. 2(a), 2(b), and 2(c), respectively, the calculated dependencies of enhancement factor β, reflectivity ρ, and SH conversion efficiency η on pump power. We set the calculation parameters to the following (realistic) values: $R_0 = 99.8\%$, $\alpha = 2.8 \times 10^{-5}\,\mathrm{W}^{-1}$, and $R_1 = 95.5\%$ (solid curves), 99.3% (dashed curves), and 99.8% (dotted curves). The first two values chosen for R_1 represent $R_1 < R_0$; the third choice corresponds to $R_1 = R_0$. We see that β, ρ, and η strongly depend on incident power P_i. Enhancement factor β monotonically decreases as P_i increases because the intracavity loss increases. Only the slope of this decrease gets steeper for larger R_1. The SH conversion efficiency η is related to α, β, and I_i by

$$\eta = \alpha \beta^2 I_i . \tag{9}$$

It follows that η first increases with increasing I_i, reaches a maximum there where $\partial\beta/\partial I_i = -\beta/2I_i$, and thereafter decreases. The position of this maximum shifts to higher pump powers for smaller R_1. Because η is not a linear function of P_i, the generated SH power P_{SH}, although it is quadratic in the intracavity power, is not quadratic in P_i. Also, the maximum value of η is not necessarily reached at the P_i that fulfills the loss-matching condition (see the dotted and dashed curves in Fig. 2). The behavior of reflectivity ρ depends on the relation between R_1 and R_0. For $R_1 \geqslant R_0$, ρ increases with increasing P_i. For $R_1 < R_0$, ρ is no longer a monotonic function of P_i; it first decreases to zero and then increases as P_i rises.

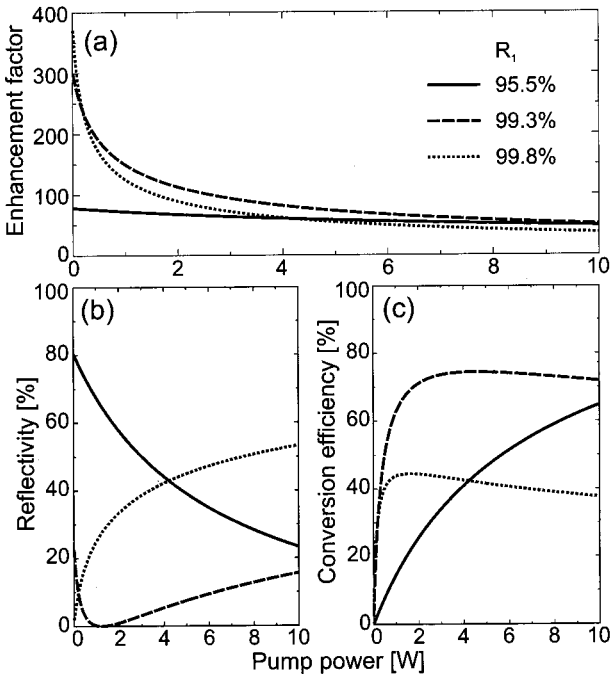

Fig. 2. Calculated (a) steady-state enhancement factor, (b) reflectivity, and (c) SH conversion efficiency as functions of fundamental power. Calculation parameters: $R_0 = 99.8\%$, $\alpha = 2.8 \times 10^{-5}\ \mathrm{W}^{-1}$; $R_1 = 95.5\%$, 99.3%, 99.8%.

The above discussion implies that the theory of an empty Fabry–Perot resonator is inadequate to describe completely the performance of a doubling cavity. Even for small pump powers, for which the losses that are due to SHG are small and the increase of SH conversion efficiency η is approximately linear in P_i, the proper theory yields significant variations of enhancement factor β and reflectivity ρ (see Fig. 2). Consequently, only simultaneous measurements of the power dependence of ρ and η permit us to characterize a doubling cavity. In particular, such measurements are required for determining both R_0 and α, which are important quantities for the strategy to select the most appropriate input coupler. While the dependence of ρ on P_i reveals the relation between R_1 and R_0, the accompanying measurement of η fixes the value of α. It is interesting to note here that the theory of an empty Fabry–Perot resonator is able to imitate the cavity performance at one pump power. From the measured reflectivity an apparent loss, i.e., R_0, can be inferred by means of Eq. (8) and used to determine the corresponding enhancement factor from Eq. (7). This enhancement factor and the measured SH power then lead to a value for α. For another pump power, however, the values of R_0 and α will be different. Hence this treatment leads to inconsistent results.

There is one more thing that we have to include in the model to obtain quantitative agreement with the experiment. The above argument, although it is valid on a qualitative level, assumes a truly single-frequency excitation of the cavity. A realistic laser, however, always produces an output that exhibits a distribution of frequencies with a finite width (including both the intrinsic width and the frequency jitter). Therefore, in what follows, we incorporate the frequency distribution of the incident laser field represented at a given fundamental frequency ω by $E_i(\omega)$. Similarly, the intracavity and reflected fields are denoted, respectively, $E_c(\omega)$ and $E_r(\omega)$. To calculate these fields we make use of Eqs. (3) and (5) with the added dimension that also waves with frequencies detuned from the true resonance are incident into and exist in the cavity. The two equations through which the SHG process enters our model, Eqs. (1) and (2), should be slightly reformulated to account for mutual interaction between fields at different frequencies. First, the intensity at harmonic frequency Ω is given by

$$I_{\mathrm{SH}}(\Omega, n) = \tfrac{1}{2}\epsilon_0 c\,\alpha \left| \int_{-\infty}^{+\infty} E_c(\Omega - \omega, n) E_c(\omega, n)\,\mathrm{d}\omega \right|^2 . \tag{10}$$

We still refer to this nonlinear process as SHG, even though Eq. (10) describes sum-frequency generation. However, we assume that the typical width of the frequency distribution of incident field $\delta\omega$ is many orders of magnitude smaller than central frequency ω_0 (usually $\delta\omega/\omega_0 \approx 10^{-9}$). Second, the crystal transmissivity $T_{\mathrm{SH}}(n)$ that accounts for the intensity-dependent loss is still given by Eq. (2), though for completeness we write

$$T_{\mathrm{SH}}(n) = 1 - \tfrac{1}{2}\epsilon_0 c\,\alpha \int_{-\infty}^{+\infty} |E_c(\omega, n)|^2\,\mathrm{d}\omega. \tag{11}$$

Because the coupling strength between two fields at different frequencies is proportional to the product of the associated optical intensities, $T_{\mathrm{SH}}(n)$ depends only on the integrated intracavity intensity. It is thus independent of Ω and, consequently, of ϕ.

The consequence of including the laser mode profile in the model is crucial for the cavity performance. The shape of this profile and also its width $\delta\omega$ strikingly influence cavity reflectivity ρ, enhancement factor β, and SH conversion efficiency η. In general, the broader the laser spectrum is, the higher is ρ and the lower are β and η. This is a consequence of the fact that the cavity mode exhibits a finite full width at half-maximum (FWHM) $\delta\omega_c$ and acts therefore as a bandpass filter. Whereas for $\delta\omega \ll \delta\omega_c$ the assumption of single-frequency excitation of the cavity is satisfactory, for $\delta\omega \gg \delta\omega_c$ the cavity prevents almost the whole laser spectrum from entering the cavity.

A particular doubling cavity is optimized when the proper choice of input coupler reflectivity R_1 is made. The main goal here is therefore to ascertain the values of R_0 and α and to determine the profile of the laser mode (including $\delta\omega$). Only when all these parameters are known can we select R_1 by employing the model presented above.

3. SETUP

In Fig. 3 we show a schematic of our experimental setup. The fundamental beam at 850 nm is produced from a single-frequency Ti:sapphire laser (pumped with a 10-W, 532-nm, diode-pumped frequency-doubled Nd:YVO_4 laser) with its mode referenced to a thermally isolated cavity. A fundamental power of as much as 1.7 W is available from this system. The doubling cavity is a four-mirror ring resonator. Its geometry was proposed by use of a ray tracing algorithm and optimized during the alignment procedure. The SH radiation is generated in the crystal in single pass. We use a LBO crystal with dimensions 4 mm × 4 mm × 10 mm that is Brewster cut and phase matched for 850 nm. Type I critical phase matching is employed because at our wavelength it is the most efficient type. The phase-matching angles are $\theta = 90°$ and $\varphi = 26.9°$. The infrared light is coupled into the doubling cavity through plane mirror M1 with reflectivity R_1. Five mirrors, with $R_1 = 95.5\%$, 97.3%, 98.5%, 98.7%, 99.7% (for 850 nm) were used in our experiments. The next mirror, M2, is also plane and is high-reflection coated for 850 nm. M2 is mounted upon a piezoelectric transducer (PZT) that provides at maximum a displacement of 10 μm. The last two cavity mirrors, M3 and M4, are both concave with a radius of curvature of 10 cm. They are also high-reflection coated for 850 nm. To ensure mechanical stability all mirrors and also the crystal are connected to a monolithic cavity block made from high-strength aluminum. M3 and M4 are mounted upon differential screws, and their alignment can thus be tweaked with high precision. The crystal is placed on a stage that allows for two angular adjustments and has all three translational degrees of freedom. Two lenses, L1 and L2, are used for mode matching of the fundamental beam into the cavity. They are both antireflection coated for 850 nm. The focal lengths of L1 and L2 are −5 and 10 cm, respectively. The separation between these lenses can be adjusted; L1 is mounted upon a translator.

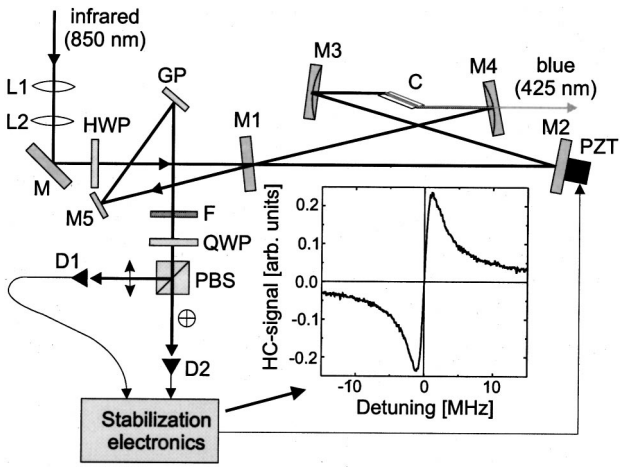

Fig. 3. Schematic design of the doubling cavity: L1, L2, mode-matching lenses; M, folding mirror; HWP, half-wave plate; M1, input coupler; M2, PZT-driven mirror; M3, M4, concave mirrors; C, LBO crystal; GP, glass plate; M5, folding mirror; F, neutral-density filter (10%); QWP, quarter-wave plate; PBS, polarization beam splitter; D1, D2, photodiodes. Data plot, measured Hänsch–Couillaud signal as a function of the detuning of a 1-W, 850-nm fundamental beam from the cavity resonance.

To lock the cavity length onto the laser frequency we implement the Hänsch–Couillaud stabilization scheme.[12] To this end, a half-wave plate for the fundamental beam is mounted in front of M1. Only p polarization is supported by the cavity because of the Brewster-cut crystal. A small nonresonant s component is obtained by rotation of the half-wave plate slightly. This s component serves as a reference for the stabilization unit. The incident beam is reflected from M1 onto an aluminum-coated mirror and then onto a glass plate with a matte back face. Thereafter it passes through a neutral-density filter with a 10% transmissivity to reduce the optical power to a reasonably low level. The optics for getting a dispersion signal around the cavity resonance consists of a quarter-wave plate and a polarization beam splitter. The quarter-wave plate's axis is at an angle of 45° with respect to the polarization of the fundamental laser beam reflected at resonance. The difference between the signals detected on the two photodiodes is a measure of the phase change of the p-polarized fundamental field on reflection from the cavity. In Fig. 3 a dispersion signal as measured for a 1-W, 850-nm pump and $R_1 = 95.5\%$ is shown. After the cavity was locked to this signal, the SH power fluctuations were below $\pm 0.75\%$. Such power stability was achieved for all available input couples. It should be noted, however, that the higher the value of R_1, the narrower the dispersion feature and the more susceptible the cavity is to instabilities and the electronics to the gain settings.

For spectroscopic applications it is interesting to discuss the range of tunability of the SH frequency. The total (optical) length of a single-cavity round trip was measured to be 632 mm. This implies that the free spectral range (FSR) is ≃474 MHz. To change the resonance frequency by $\delta\nu$ requires that cavity length L be changed by $\delta L = -\lambda\,\delta\nu/\mathrm{FSR}$, where λ is the fundamental wavelength. Now, because PZT-driven mirror M2 can move at maximum $\pm 5\ \mu$m, the cavity can be scanned continuously with the laser for no more than ± 2.8 GHz at 850 nm. This scan range corresponds to a change in the SH frequency of ± 5.6 GHz. In practice, we could accomplish a change of only ± 3 GHz at 425 nm.[13] For larger wavelength ranges, discontinuous frequency steps are required. Moreover, for a step of more than 0.2 nm at the fundamental wavelength, the cavity alignment (especially the orientation of the LBO crystal) must be adjusted. We measured a drastic decay of the SH power below 840 and above 880 nm. At these two wavelengths, however, we still could optimize the SH power at, respectively, 30% and 50% of its best measured value at 850 nm.[14]

The direct SH beam exiting the doubling cavity through mirror M4 contains 77% of the total generated SH power. The main loss is caused by the output face of the LBO crystal, which is Brewster cut for 850 nm. For the s-polarized 425-nm beam the reflectivity of the crystal is 16.6%. This reflected light is also coupled out of the cavity and can be used in an experiment. The last source of loss is mirror M4, with a transmissivity at 425 nm of 92.7%. We must also note that the direct SH beam is astigmatic because of the phase-matching process in LBO. The measured beam divergence was 12 mrad in the horizontal and 3.5 mrad in the vertical directions. In both of these directions the intensity profile is to a good approximation described by a Gaussian function.

4. EXPERIMENT AND ANALYSIS

To optimize the doubling cavity by selecting the most suitable input coupler we must first ascertain the intensity-independent loss, expressed here as R_0, SH coefficient α, and also the profile and frequency width $\delta\omega$ of the laser mode. To get a reliable estimate of α and R_0 we used the input coupler with the highest transmissivity ($R_1 = 95.5\%$). For this choice we expected $\delta\omega$ to be considerably smaller than the FWHM of the cavity mode, $\delta\omega_c$, which is certainly larger than $2\pi \times 3.4$ MHz (this frequency width would be seen for $R_0 = 100\%$ and $\alpha = 0$). The assumption that $\delta\omega \ll \delta\omega_c$ implies that the laser mode can, to a good approximation, be treated as a truly single-frequency excitation of the cavity. We then measured the dependence of reflected fundamental power P_r and also of the total generated SH power P_{SH} on incident power P_i at 850 nm.[15] These dependencies are shown by squares in Figs. 4(a) and 4(b), respectively. We could reproduce both of them simultaneously with our model only for $R_0 \simeq 99.8(1)\%$ and $\alpha \simeq 2.7(1) \times 10^{-5}\ \mathrm{W}^{-1}$. Another way to identify the value of α relies on measurements of P_{SH} as a function of intracavity fundamental power P_c. To this end we determined the transmissivity of mirror M4 for 850 nm to be $T_4 \simeq 0.0028\%$ and measured transmitted fundamental power P_t ($=T_4 P_c$). The dependence of P_{SH} on P_t was quadratic, and a least-squares fit to it revealed $\alpha = 2.8(1) \times 10^{-5}\ \mathrm{W}^{-1}$, in excellent agreement with the value obtained above.

Using the estimated values of R_0 and α, we could calculate the cavity mode for the input coupler with the highest reflectivity, $R_1 = 99.7\%$. The FWHM width of this mode, $\delta\omega_c$, was $2\pi \times 830$ kHz at a 1-W pump (the cavity mode gets broader at higher incident power because the overall loss increases as a result of SHG). Unfortunately, we could not make use of this narrow cavity mode to determine the laser mode profile while scanning the cavity across the free spectral range. At low scanning frequencies (<5 kHz) acoustic noise was coupled to

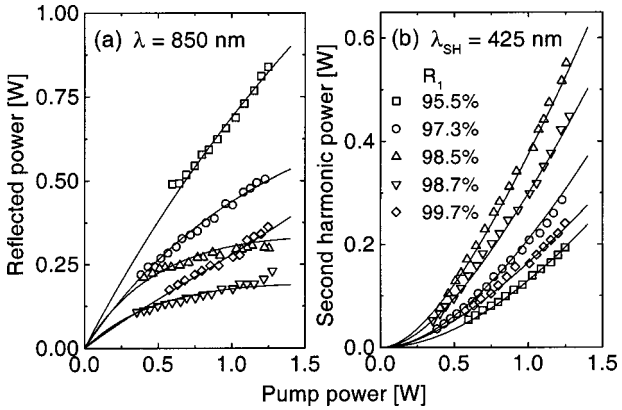

Fig. 4. Steady-state dependence of (a) the reflected fundamental power and (b) the total SH power on the incident pump power for $R_1 = 95.5\%$, 97.3%, 98.5%, 98.7%, and 99.7%. Solid curves, modeled dependencies.

the cavity, whereas at high frequencies (>5 kHz) dynamic effects started to play a role. This result becomes obvious when one recognizes that at a 5-kHz frequency the cavity mode is scanned through in only ~350 ns, whereas it takes ~1 μs to reach the steady state. Therefore we made use of the static measurements with this mirror (shown in Fig. 4 as diamonds) and guessed the laser mode profile. The best agreement with the experiment was obtained when we assumed a parabolic distribution of the incident laser intensity $I_i(\omega)$ around the central frequency ω_0:

$$I_i(\omega) \propto 1 - \left(\frac{\omega - \omega_0}{\delta\omega/\sqrt{2}} \right)^2, \tag{12}$$

with the FWHM frequency width $\delta\omega/2\pi \simeq 660$ kHz and $|\omega - \omega_0| \leqslant \delta\omega/\sqrt{2}$ [and otherwise $I_i(\omega) = 0$]. We note that such a profile is a reasonable assumption for a single-mode laser.

Now, having the estimates for all crucial parameters, our model predicted the best performance for the input coupler with $R_1 = 98.5\%$. The experimental results for this input coupler are shown in Fig. 4 as upward-pointing triangles. They clearly confirm this prediction and demonstrate the strength of the analysis presented. For completeness and to improve the values of R_0, α, and $\delta\omega$ we measured the power dependencies for two additional input couplers with $R_1 = 97.3\%$ and 98.7%. These are also shown in Fig. 4. All acquired data sets were then fitted simultaneously to the model by a least-squares deviation algorithm. The free-fit parameters were R_0, α, and $\delta\omega$, whose final values are $R_0 = 99.8(1)\%$, $\alpha = 2.80(5) \times 10^{-5}$ W^{-1}, and $\delta\omega/2\pi = 630(50)$ kHz. The curves in Fig. 4 present the modeled dependencies. These are in excellent agreement with the experiment. We must mention that only with the laser mode profile from Eq. (12) were we able to bring the model into agreement with the data, although a number of other distributions were also tried. For example, Lorentzian and Gaussian line shapes, which correspond to the same measured SH conversion efficiency, led to considerably higher cavity reflectivity than observed. The narrower the cavity mode, the more pronounced this discrepancy. This result implies that a doubling cavity can be employed as a device for indirect characterization of the spectrum of a single-mode laser.

The accuracy with which R_0 and $\delta\omega$ were determined demonstrates that the cavity is extremely sensitive to any changes in these quantities and, therefore, also to alignment and mode matching. All data presented in Fig. 4 were obtained in a relatively short span of time (a few hours) to ensure identical experimental conditions. In general, the conversion efficiency obtained from the cavity fluctuates from day to day on a level of ~10%. Whereas the results from Fig. 4 can routinely be attained, they do not represent the best performance that we achieved. The highest SH power and conversion efficiency obtained with the optimal input coupler ($R_1 = 98.5\%$) are presented in Figs. 5(a) and 5(b), respectively. At maximum, 53(3)% of the fundamental power was converted to SH power: A 1.54(4)-W pump resulted in 820 ± 20 mW of blue light, which implies an intracavity power

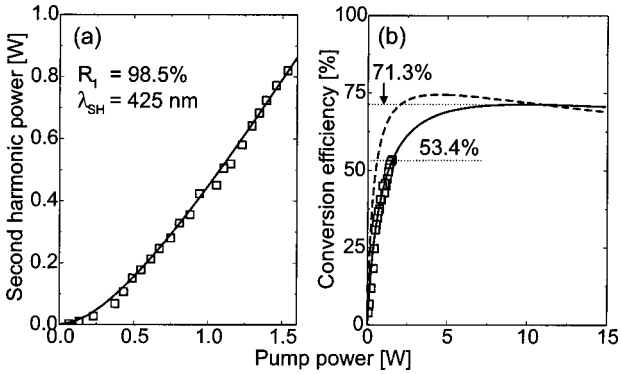

Fig. 5. Best achieved performance: (a) SH power and (b) conversion efficiency as functions of incident fundamental power. Squares, measured data; solid curves, modeled dependence; dashed curve, dependence modeled with the assumption that $\delta\omega = 0$ and $R_1 = 99.3\%$ [see also the dashed curve in Fig. 2(c)].

$P_c \simeq 170$ W and consequently an enhancement factor $\beta \simeq 110$. The data from Fig. 5 are well described with our model, assuming that $R_0 = 99.9\%$, $\alpha = 2.8 \times 10^{-5}$ W^{-1}, and $\delta\omega/2\pi \simeq 450$ kHz. We attribute the observed changes in R_0 and $\delta\omega$ to the behavior of the Ti:sapphire laser that turned out to be the main source of long-term fluctuations. The sensitivity of the cavity to these fluctuations is less pronounced as the transmissivity of the input coupler increases. Therefore for a given application a compromise must be found between sacrificing the SH power and maintaining its long-term stability. It is also interesting to compare the data from Fig. 5 with the theoretical results obtained with the assumption that $\delta\omega = 0$ [the dashed curve in Fig. 5(b)]. This comparison shows that the conversion efficiency could be optimized even at a considerably higher level, provided that a laser that exhibits a narrower mode were used.

Heretofore we have demonstrated the ability of our model to describe a cavity in the steady-state regime. Now we briefly discuss the transient behavior of the cavity. Such a study was carried out earlier by, for example, Lawrence *et al.*,[11] who investigated the dynamic response of an empty optical resonator. In their experiment, either the laser frequency or the cavity mode was scanned. The transient effects were detected on the measured spectrum of the transmitted and reflected light and also on the Pound–Drewer–Hall signal.[14] In contrast, we kept the cavity resonant with the laser and used an acousto-optic modulator with a 50-ns rise time to turn the incident beam OFF and ON. The ON period was adjusted to 3 μs, and the switching frequency to 250 kHz. The cavity regulation electronics does not respond to this frequency and thus detects only the mean Hänsch–Couillaud signal. Although the shape of this signal was influenced by the transients of the reflected field, we could still balance the detection scheme to maintain the cavity resonance. The reflected and the SH powers were each detected with a photodiode with a 0.5-ns rise time. For illustration, in Fig. 6 our measurements with three input couplers—$R_1 = 95.5\%$ (solid curves), 98.5% (dashed curves), and 99.7% (dotted curves)—are shown for a 1.25-W, 850-nm pump [for a lower (higher) incident power the dynamics is slightly slower (faster)]. These data were obtained by av-

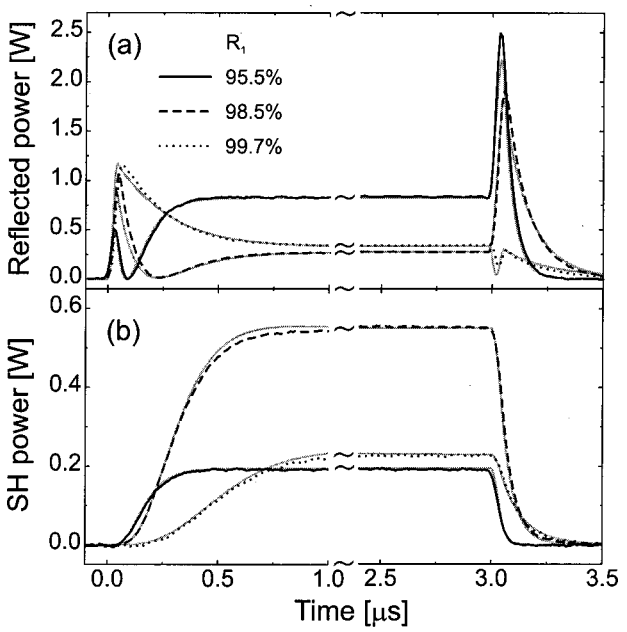

Fig. 6. Comparison of measured and calculated transients of the cavity for a 1.25-W, 850-nm pump: (a) reflected fundamental power and (b) SH power. $R_1 = 95.5\%$, 98.5%, 99.7%. Lighter solid curves, modeled time dependencies.

eraging 32 times with a digital oscilloscope. The calculated time dependencies, shown in Fig. 6 as lighter curves, reproduce all the measured transients simultaneously for $R_0 = 99.7(1)\%$, $\alpha = 2.8(1) \times 10^{-5}$ W^{-1}, and $\delta\omega/2\pi = 550(60)$ kHz. These parameters are, within the errors, identical to those reported above. The excellent agreement between the measured and the modeled cavity dynamics again demonstrates the strength of our approach to SHG in an external enhancement resonator.

5. CONCLUSION

We have presented an extensive theoretical and experimental investigation of an external enhancement resonator for second-harmonic generation. We introduced a theoretical model that takes into account the fact that the cavity losses increase as a result of an increase of second-harmonic conversion efficiency as the intracavity intensity builds up. Interestingly, although this argument is fairly trivial and has amazing consequences, (to the best of our knowledge) no one has included it in studies of resonant frequency doubling so far. Only by incorporating this essential feature can the intriguing behavior of a doubling cavity correctly be reproduced and predicted. Furthermore, to obtain a quantitative agreement with the experiment requires that the true shape of the laser spectrum also be considered. We have seen excellent agreement between the proposed model and measurements with a lithium triborate-based doubling cavity for SHG of a single-frequency Ti:sapphire laser at 850 nm. This model accurately reproduces the cavity performance in both steady-state and transient regimes. The effective SH coefficient, the intensity-independent loss, and the laser mode profile were identified as the factors that ultimately limit cavity performance. They were all successfully extracted from the data and used to determine the optimum reflectivity of the input coupler. We maximized the SH conversion efficiency at a 53% level for a 1.54-W fundamental power and have seen that, in our case, the most limiting factor of all is the relatively broad laser line.

The framework presented here provides the means for pushing the performance of a doubling cavity to its ultimate limits within the technical constraints that one faces in reality (no laser line is infinitely sharp, no mirror-coating technique is perfect, etc.). Moreover, it should also prove useful for analyzing the process of resonant sum-frequency mixing with single-mode lasers. The extreme sensitivity of the power reflected from the cavity to changes in the total cavity loss, seen in both static and transient regimes, indicates that high-quality cavities locked to a single-mode laser can be used as an alternative approach to conventional cavity ring-down spectroscopy.

ACKNOWLEDGMENTS

The authors thank P. Dolron, R. van Dongen, and N. van Wijk for technical support and assistance. Part of this research was supported by the Stichting voor Fundamenteel Onderzoek der Materie, which is financially supported by the Nederlandse Organisatie voor Wetenschappelijk Onderzoek.

J. Hohlfeld's e-mail address is hohlfeld@sci.kun.nl.

REFERENCES AND NOTES

1. P. A. Franken, A. E. Hill, C. W. Peters, and G. Weinreich, "Generation of optical harmonics," Phys. Rev. Lett. **7**, 118–119 (1961).
2. J. A. Armstrong, N. Bloembergen, J. Ducuing, and P. S. Pershan, "Interactions between light waves in a nonlinear dielectric," Phys. Rev. **127**, 1918–1939 (1962).
3. A. Ashkin, G. D. Boyd, and J. M. Dziendzic, "Resonant optical second harmonic generation and mixing," IEEE J. Quantum Electron. **QE-2**, 109–124 (1966).
4. C. S. Adams and A. I. Ferguson, "Tunable narrow linewidth ultra-violet light generation by frequency doubling of a ring Ti:sapphire laser using lithium tri-borate in an external enhancement cavity," Opt. Commun. **90**, 89–94 (1992).
5. S. Bourzeix, M. D. Plimmer, F. Nez, L. Julien, and F. Biraben, "Efficient frequency doubling of a continuous wave titanium:sapphire laser in an external enhancement cavity," Opt. Commun. **99**, 89–94 (1993).
6. H. Tsuchida, "Frequency doubling of tunable Ti:sapphire laser with $KNbO_3$ in external cavity," Jpn. J. Appl. Phys., Part 1 **33**, 6190–6194 (1994).
7. S. Bourzeix, B. de Beauvoir, F. Nez, F. de Tomasi, L. Julien, and F. Biraben, "Ultraviolet light generation at 205 nm by two frequency doubling steps of a cw titanium-sapphire laser," Opt. Commun. **133**, 239–244 (1997).
8. T. Fujii, H. Kumagai, K. Midorikawa, and M. Obara, "Development of a high-power deep-ultraviolet continuous-wave coherent light source for laser cooling of silicon atoms," Opt. Lett. **25**, 1457–1459 (2000).
9. G. D. Boyd and D. A. Kleinman, "Parametric interaction of focused gaussian light beams," J. Appl. Phys. **39**, 3597–3639 (1968).
10. Throughout this paper we follow the usual convention that both the reflectivity and the transmissivity are related to the optical intensity (power).
11. M. J. Lawrence, B. Willke, M. E. Husman, E. K. Gustafson, and R. L. Byer, "Dynamic response of a Fabry–Perot interferometer," J. Opt. Soc. Am. B **16**, 523–532 (1999).

12. T. W. Hänsch and B. Couillaud, "Laser frequency stabilization by polarization spectroscopy of a reflecting reference cavity," Opt. Commun. **35**, 441–444 (1980).
13. To get a continuous scan range larger than ±3 GHz, one could mount a Brewster plate into the cavity. It could then take care of slow variations while the PZT-driven mirror would correct for higher frequencies.
14. The Hänsch–Couillaud stabilization method is not suitable for spectroscopic applications, especially when a broad wavelength range is required. In carrying out the wavelength tuning measurements we applied the Pound–Drewer–Hall stabilization scheme [see R. W. P. Drewer, J. L. Hall, F. V. Kowalski, J. Hough, G. M. Ford, A. J. Munley, and H. Ward, "Laser phase and frequency stabilization using an optical resonator," Appl. Phys. B **31**, 97–105 (1983)]. The power stability with both of these two techniques remained the same (at least within the limit that we could detect).
15. Absolute power values are uncertain to ±2.5% of the stated value because of uncertainty in detector calibration.